Heavy-Particle Energy-Loss Spectrometry: Inelastic Cross Sections for Protons Incident upon Helium†

John T. Park and F. D. Schowengerdt

Physics Department, University of Missouri-Rolla, Rolla, Missouri 65401
(Received 21 May 1969)

A method is described whereby absolute cross sections are obtained from inelastic energy-loss spectra induced by ions incident upon gaseous targets at energies of 25–125 keV. Inelastic energy-loss spectra of helium for proton impact are presented. Apparent differential cross sections and absolute total cross sections are obtained from the spectra. Total cross sections for the sum of the $1^1S \rightarrow 2^1S$ and $1^1S \rightarrow 2^1P$ excitations are reported, along with estimates of the relative contributions of each. Total ionization cross sections, total cross sections for inelastic scattering, apparent energy distributions of ejected electrons, and partial ionic stopping powers are also reported. The excitation cross sections show excellent agreement with recent calculations on the coupled-state approximation. The ionization cross sections show good agreement with results obtained by other methods, except at the lower impact energies. The apparent energy distributions of ejected electrons fall below the results of direct measurements and show poor agreement with the available theory.

I. INTRODUCTION

Traditional methods of measuring cross sections for heavy-particle collision processes involving 25 – 125 keV ions have focused attention on the secondary products of the collision. Thus, detection of the slow ions or ejected electrons has been the primary means available for measuring ionization cross sections, while detection of radiation from collisionally excited states has been relied upon for excitation cross sections.

The conventional method of measuring total ionization cross sections is the parallel-plate condenser method. The method has been used extensively by Gilbody and Lee,[1] Gilbody *et al.*,[2] Federenko *et al.*,[3] and DeHeer *et al.*,[4] among others. Most of the secondary effects have been eliminated or corrected for in the recent work. The presence of neutrals in beam, however, is a potential source of error which is difficult to evaluate. While corrections to the total beam currents can be made by measuring the neutral component, its contribution to the ionization current is usually estimated.[4] Other errors arise from the fact that the measured cross sections depend on ratios of currents collected by different electrode configurations and therefore, depend on the relative collection efficiencies. Recombination of the slow ions and ejected electrons is another possible factor. Discrepancies between the results of different investigators, particularly at energies below 40 keV, suggest the importance of the above effects in measurements by this method.

Recently, measurements of energy and angular distributions of the electrons ejected in ionizing collisions has become an important means of obtaining information about the collision. Ejected electron spectra have been studied by Berry,[5] Kuyatt and Jorgensen,[6] and Rudd *et al.*,[7] among others. These experiments have the important advantage that differential cross sections are measured directly. They suffer, however, from disadvantages common to the parallel-plate experiments in that beam composition and recombination must be considered and that the cross sections depend on absolute current measurements. An additional difficulty arises in collecting electrons ejected in the forward direction.

In the case of excitation cross sections, the commonly used experimental methods possess even more uncertainties than those discussed above. Essentially, the only methods previously available have been those in which radiation from excited target atoms is measured. The literature has been reviewed by Fite[8] and DeHeer.[9] Among the examples of the method to be found in the literature are the experiments of DuFay *et al.*,[10] Moussa *et al.*,[11] and Thomas and Bent.[12] Effects of cascading from higher-order excited states and imprisonment of resonance lines are commonly cited difficulties.[8,9] Imprisonment of the 584 Å resonance line in helium, for example, has thus far prevented measurement of the cross section for excitation of the 2^1P state by optical methods. Still, the major source of uncertainty in optical experiments lies in determining detector efficiencies. Thomas,[12] for example, reports systematic disagreement of as much as 150% in results of the various experiments.

The difficulties encountered in all of the experi-

ments discussed above can be attributed to two factors: (a) detection and analysis is performed on secondary products of the collision, and (b) the measured cross sections depend on detector efficiencies. Because of the former, events which occur in the ion beam before the collision and among the product particles after the collision can introduce errors in the measurements. Because of the latter, accurate absolute measurements are difficult to perform.

The method to be described here, which is an extension of the techniques of photoabsorption and electron spectrometry, involves detection and analysis of the primary beam particles only. The disturbing effects of post-collision events are thus eliminated. With sufficient resolution, cross sections differential in energy loss can be obtained from a study of the inelastic energy-loss spectra induced by the forward-scattered beam. The cross sections are independent of detection efficiency. If the collision process, or processes, responsible for the energy losses within a given range can be identified, the corresponding total cross sections can be obtained by integrating the differential cross sections over that range. The amount of detail in the differential cross sections and hence, the degree of certainty with which individual processes can be identified is limited only by the instrumental resolution.

II. METHOD

The method used here consists in sending a beam of accelerated ions through a target gas, mass analyzing the forward-scattered beam, then decelerating the selected ions to a low well-defined energy for energy analysis and detection.

An over-all schematic diagram of the apparatus is shown in Fig. 1. The apparatus has been described in detail elsewhere.[13] Ions of charge q are formed in a plasma ion source. The ions are focused and accelerated through a potential $V + V_0 + \Delta V$, where V is the output of the high-voltage power supply (25 – 250 kV), V_0 is a precision offset voltage (2 kV), and ΔV is a sweep voltage, continuously variable from -180 to $+180$ V.

The incident ions have a distribution of kinetic energies about the value $q(V + V_0 + \Delta V)$, the distribution being that of the energy of formation of the ions in the source. With no gas in the target chamber the beam is collimated by the chamber apertures, is momentum analyzed by the magnet, and then decelerated through a potential V. Therefore, the ions arrive at the energy analyzer with a distribution of energies about the value $q(V_0 + \Delta V)$. The electrostatic analyzer is of the 127°-focusing design. The sweep voltage ΔV is now set to zero, and the analyzer plate voltage is adjusted for a maximum detected current. That is, the analyzer is set to accept particles of energy qV_0. Owing to the finite resolving power of the analyzer, a small distribution of energies about qV_0 is also accepted. The sweep voltage ΔV is slowly varied and a plot of detected current versus $q\Delta V$ is traced out on an X-Y recorder located at ground potential. The signals are fed to the recorder by means of null-balancing servomechanisms. Detection and measurement of the current is accomplished by a 15-stage particle multiplier and electrometer, respectively. The plot obtained here (hereafter referred to as the resolution function Φ) is a superposition, or convolution, of the source distribution and the dispersive effects introduced by the apparatus. The function Φ is proportional to the current detected with no gas in the target chamber. It represents the interaction of the entire instrument with the initial ion-beam energy distribution.

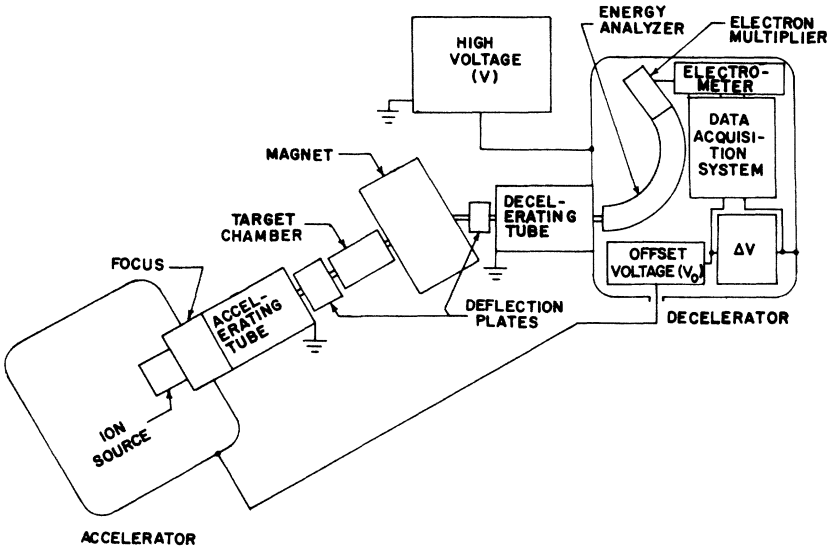

FIG. 1. Schematic drawing of the apparatus.

Gas is now introduced into the target chamber and ΔV is again swept. No other experimental parameters are changed from their settings in the gas-out condition. Because of this the incident-ion energy distribution and the effects of the apparatus on it are unchanged. The spectrum now obtained is a convolution of the incident-ion energy distribution with the energy and angular effects from the apparatus and from the target gas. The energy-loss spectrum (hereafter referred to as R) is proportional to the current detected with n atoms/cm^3 of gas in the target chamber.

Since the two functions R and Φ are plotted under the same experimental conditions, with only the introduction of gas into the target chamber distinguishing them, the following relationship holds:

$$R(\xi) = ndx \int \Phi(\xi - \xi') \frac{d\bar{\sigma}(\xi')}{d\xi} d\xi', \tag{1}$$

where $$\frac{d\bar{\sigma}}{d\xi} \equiv \int_{\Delta\Omega} \frac{d^2\sigma(\theta, \xi)}{d\Omega d\xi} d\Omega,$$

$d^2\sigma/d\Omega d\xi$ is the doubly differential cross section per unit angle and energy loss, for scattering into the solid angle $d\Omega$, and energy-loss interval $d\xi$, ξ is a (positive) energy loss as measured from the most probable energy of the beam particles, $\Delta\Omega$ is the solid angle defined by the instrumental acceptance angles, θ is the laboratory scattering angle, n is the number density of scatterers, and dx is the effective path length for scattering.

The observed functions R and Φ are functions of energy loss only. This has been established experimentally by showing that the incident current and the current detected directly in front of the energy analyzer are unaffected by sweeping ΔV over the energy-loss range (360 eV). The observed currents are constant to within 1% over a range exceeding 3 times that used for the sweep.[13] These tests show that the energy dependence of the apparatus function arises solely from the energy analyzer, the magnet acting only as a mass analyzer in this mode. They also indicate that angular effects of the deceleration process are constant over the spectral energy-loss range.

The experimental cross section appearing in Eq. (1) is equivalent to the energy-loss differential cross section to the extent that

$$\frac{d\bar{\sigma}(\xi)}{d\xi} = \int_{4\pi} \frac{d^2\sigma(\theta, \xi)}{d\Omega d\xi} d\Omega = \frac{d\sigma(\xi)}{d\xi}.$$

For these equalities to hold, the fraction of the beam scattered beyond the acceptance angle of the apparatus ($\simeq 10^{-3}$ rad.) by the target gas must be negligible. That such is the case may be shown experimentally by accounting for all of the beam in both the absence and presence of target gas. The experimental condition which assures that essentially all of the scattered current contributing to the cross section of interest has been detected is

$$\int R(\xi)\, d\xi \Big/ \int \Phi(\xi)\, d\xi + \sigma_c ndx \simeq 1, \tag{2}$$

where σ_c is the cross section for all charge-changing processes. (The instrument discriminates against any projectile which changes charge.) With the exception of σ_c, all quantities here are directly measurable. The charge-exchange cross section may be obtained from theory or the experimental data of others.

Equation (2) has been used in an experimental determination of the effects of angular scattering of protons by helium. The functions R and Φ were integrated numerically and the charge-exchange cross sections were obtained from the data of DeHeer *et al.*[4] These agree to within 10% of the earlier data of Stier and Barnett[14] and the theoretical calculations of Mapleton.[15] The results indicate that the above equality is satisfied within our experimental accuracy. Estimates of the fraction of the beam scattered beyond the acceptance angle using this method average 3% with both positive and negative fluctuations observed. No trend with energy was detected. Barat and Houver[16] have reported cross sections differential in angle only for protons on various inert gases. In the case of helium, Barat finds the cross section dropping two orders of magnitude in a region of 0.05 deg (8×10^{-4} rad) about the forward direction for protons incident at 80 keV. These data are consistent with the results discussed above.

To determine absolute cross sections, it will be necessary to assume that the elastic and inelastic collision cross sections are separable and that the small fraction of the ions scattered out of the acceptance angles do not produce energy-loss spectra which differ greatly from that produced by the forward-scattered beam. If large-angle scattering events can produce significant changes in the spectra, then these events, although statistically rare, could introduce uncertainties in the cross sections measured by this method.

The experimental cross section given by Eq. (1) has thus been shown to be essentially equal to the differential cross section $d\sigma/d\xi$ by virtue of the experimentally observed fact that the number of particles scattered beyond the acceptance angles of the instrument is small compared with the number of particles passed by the instrument, at least in the case of protons incident on helium. The bar on the differential cross section in Eq. (1) can, therefore, be removed.

We first note two important limiting cases in the solution of Eq. (1). In case the slopes of Φ are much steeper than any slope in R, we can approximate Φ by a δ function and write

$$\frac{d\sigma(\xi)}{d\xi} = R(\xi)/ndx \int \Phi(\xi')\, d\xi' . \quad (3)$$

This corresponds to the case of a smooth ionization continuum, for example. In the other case, where $R(\xi)$ drops essentially to zero on either side of a peak, integration of Eq. (1) over ξ as well as ξ' yields the total cross section σ_j for all processes contributing to the peak in question. That is,

$$\sigma_j = \int_{\Delta\xi_j} R(\xi)\, d\xi / ndx \int \Phi(\xi)\, d\xi , \quad (4)$$

where $R = 0$ at either end of the interval $\Delta\xi_j$, over which R is nonzero.

In case neither of the above conditions is well satisfied, numerical deconvolution can sometimes be employed to separate the partially resolved peaks (see the Appendix).

III. EXPERIMENTAL PROCEDURE

In order for the method to be valid, it is essential that the energy-loss spectra $R(\xi)$ and the resolution curves $\Phi(\xi)$ be taken under identical experimental conditions. For this reason, considerable effort was spent in obtaining a stable beam, free of any abnormalities in its energy distribution or spatial structure. Misalignment of the beam anywhere in the instrument could be readily detected by the appearance of irregularities in the resolution curves. The irregularities could be minimized by improving the on-axis alignment of the beam during deceleration. It was consistently found that the same experimental conditions which produced an optimum resolution curve also produced the most intense and stable detected beam. No data were taken until the intensity of the beam detected in the energy analyzer could be maintained constant to within 5% for a half-hour or more.

Before gas was introduced into the target chamber, the resolution curve was traced out many times on an X-Y recorder to establish reproducibility of the primary energy-distribution and the background. Over-all system pressure was less than 1×10^{-6}-mm Hg at all times during operation.

The observed resolution is essentially equal to that obtained from the calculated resolving power of the analyzer, suggesting that the energy spread of the ions formed in the source contributes very little. The full width at half-maximum (FWHM) was 2 eV at the lower energies, showing a gradual increase to about 2.5 eV at the higher energies. The beam was analyzed at an energy of 2 keV in all cases.

With gas in the target chamber, the energy-loss spectra were traced out on the X-Y recorder. Several spectra were taken at each of four target-gas pressures for each energy used. Each spectrum was retraced with several electrometer gains. Pressures ranged from 1 to 4 μ ($ndx = 2 - 8 \times 10^{14}$ cm^{-2}). A resolution curve was taken with each spectrum and the two were used together in calculating the cross sections. Precautions were taken to ensure that no experimental parameters changed between the times the two curves were plotted. When such a change occured, and could be detected by the resulting change in beam intensity, the suspect spectra were discarded.

IV. ENERGY-LOSS SPECTRA

An example of the raw data for the case of protons incident upon helium at 50 keV is shown in Fig. 2. The background and the spectrum are shown in Fig. 2 at a gain 100 times that of the main peak. The background is due to residual gas in the system and reflections within the analyzer. The peaks at about 12 and 16 eV are due to residual gas. Their appearance is unaltered when the analyzer-plate voltages are changed. The peak at 70 eV, on the other hand, can be altered in shape and location by changes in the analyzer-plate voltages. It is due to a reflection within the analyzer. In any case, these background features are unaltered in size or shape by introducing gas into the target chamber and are subsequently eliminated in the course of reducing the data.

Typical energy-loss spectra for protons on helium are shown in Fig. 3 for impact energies of 25, 50, and 100 keV. The inelastic regions of the spectra are shown at a gain 100 times that of the elastic peak. The backgrounds have been subtracted from the spectra.

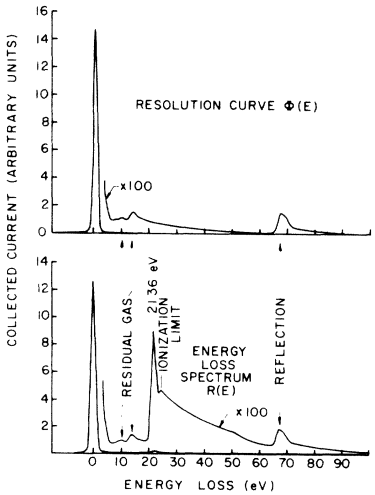

FIG. 2. Sample resolution curve and energy-loss spectrum (protons on helium, 50 keV primary energy, $ndx = 6 \times 10^{14}$ cm^{-2}).

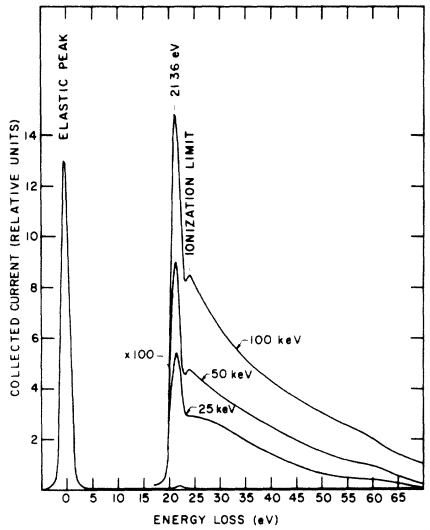

FIG. 3. Energy-loss spectra of helium for proton impact.

The first inelastic peak in the curves in Fig. 3 occurs at 21.36 ± 0.16 eV. This value is an average of the results of 12 measurements. The uncertainty is 1 standard deviation. Spectroscopic and electron-impact measurements, which are in excellent agreement, place the value of the 2^1P level in helium at 21.22 eV above the ground state.[17,18] The nearest levels are the 2^1S and 3^1P levels, the former occurring at 20.61 eV, the latter at 23.08 eV (see Ref. 18). Excitation of triplet states is forbidden for proton impacts by the spin-conservation rule.

With the present resolution it appears that the 21.36-eV peak is due mainly to excitations to the 2^1S and 2^1P levels, with lesser contributions from higher-order ^1S and ^1P levels. The effects of transitions to the higher-order levels is to produce a single peak, located slightly below the ionization limit (24.59 eV).

The only other feature discernible is a small bump at about 60-eV energy loss. This bump is believed due to energy transfers to both electrons in the helium atom. Transitions to autoionizing levels in this region have been observed in electron-impact spectra[18] and in analyses of electrons ejected by proton impacts.[19]

By using numerical deconvolution we have been able to further approach the true differential cross section. The deconvolution scheme is described in the Appendix. In order to yield a true differential cross section, the numerical solution of Eq. (1) would require an infinite number of data points from a completely noise-free spectrum. Therefore, any real numerical solution, resulting from operations on a finite number of points from an incompletely resolved spectrum with some noise content should be labeled as an "apparent" differential cross section.

Results of the deconvolution are shown in Fig. 4. The ordinate values have been divided by ndx ($= 6.09 \times 10^{14}$ cm^{-2}) so that the curves can be considered apparent differential cross sections, per unit energy range, for loss of energy ξ by the incident protons. The FWHM has been effectively reduced to about 1 eV by the deconvolution, but is still not sufficient to permit separation of the 2^1S and 2^1P peaks.

V. DIFFERENTIAL CROSS SECTIONS FOR THE CONTINUUM

The apparent differential cross section for the helium continuum at a proton energy of 100 keV is reproduced in Fig. 5, where comparison is made between the present curve and those obtained by Rudd and Jorgensen[20] and by Rudd *et al.*[7] through an energy analysis of the ejected electrons. Shown also are results of a scaled Born approximation (Rudd[7]) and the classical binary-encounter theory (Garcia[21]). The energy scale has been shifted to make the zero of the ejected-electron spectrum coincide with the ionization limit in the differential cross section.

Since conservation of energy can be expected to hold rigorously, the curves should coincide over those regions where the relationship between the energy lost by the incident proton and the energy gained by a single ejected electron is unique. If the energy can be transferred to both electrons, the relationship may or may not be unique. The consequences of autoionization would be expected to be the same in both the ejected-electron method and the energy-loss method, since the energy of the ejected electron is determined only by the characteristics of the discrete level from which it was ejected. Double ionization, on the other hand, would contribute two electrons to the ejec-

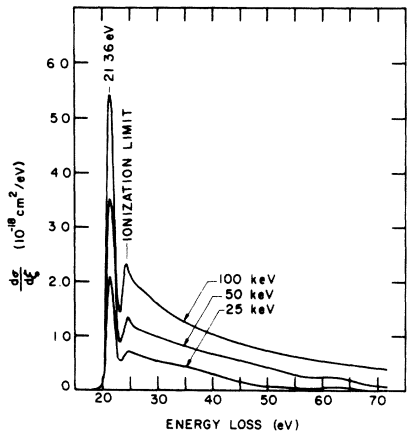

FIG. 4. Apparent energy-loss differential cross sections for protons on helium.

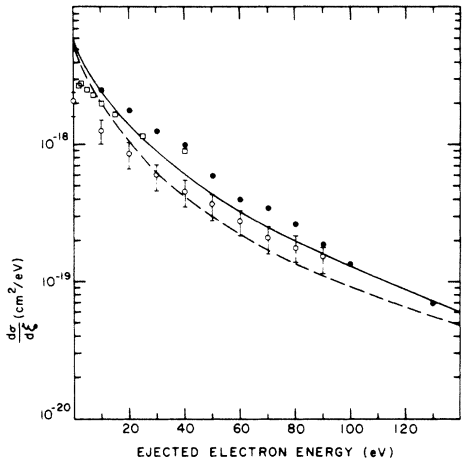

FIG. 5. Comparison of continuum region of differential cross section with ejected electron spectrum. Φ: present data; □ : ejected electron data, Rudd and Jorgensen (Ref. 20); ● : ejected electron data, Rudd *et al.* (Ref. 7); ___ scaled born approximation (Ref. 7); --- classical binary-encounter theory, Garcia (Ref. 21).

ted-electron spectrum, each having a lower energy than would be the case if all the available energy were spent in single ionization. Double ionization would simply produce a second continuum in the energy-loss spectrum. In the case of simultaneous excitation and ionization, the ejected electron would have a lower energy than would be expected in the absence of excitation, while the energy-loss spectrum would show another continuum beginning at the sum of the energy losses corresponding to the first ionization potential and the excitation potential of the level in question. The over-all effects of these two-electron processes would be to contribute more low-energy electrons to the ejected-electron spectrum and to produce features near the second ionization potential in the energy-loss spectrum. Therefore, we could expect the ejected-electron distribution to have a steeper slope than the energy-loss spectrum at low ejected-electron energies, and we could also expect some disagreement at ejected-electron energies around 30 eV.

The experimental data in Fig. 5 show suggestions of the effects discussed above. The shape of all three curves deviates from the theoretical curves as the ionization limit is approached, where the theoretical results lie a factor of 3 above the present results. This region of the curve is not readily accessible to study by the ejected-electron method because of the difficulty of making accurate measurements on slowly moving electrons.

The results of Rudd *et al.*[7] are 20 - 100% higher than the present results, showing better agreement at the higher ejected-electron energies. The effects of the two-electron processes discussed earlier cannot account for this discrepancy. The results of Rudd and Jorgensen[20] show better agreement at all energies. Rudd *et al.* have noted[7] that their integrated cross sections are systematically 28% higher than total ionization cross sections measured by others. In view of the basic differences in experimental approach, it appears that these two complementary methods yield compatible results.

VI. TOTAL EXCITATION CROSS SECTIONS

The first peak in the deconvoluted spectrum is resolved well enough to permit integration for the total cross section for processes contributing to the peak. Since the reproducibility of the raw spectra was very good ($\pm 5\%$), and the noise content low, it was not considered necessary to deconvolute all the spectra. Instead, one spectrum taken with 3 μ target gas pressure, at each primary energy, was deconvoluted and the total cross sections for excitation of the first peak were obtained by integrating over the peak in the resulting spectra. Cross sections were obtained directly from the peak heights in all the spectra (at least three taken at each of four target gas pressures; 1–4 μ) and the results were normalized to the results obtained from the deconvoluted spectrum at each energy. This procedure is a compromise between accuracy and computer time, but should involve little error since the cross section for any process is expected to be pressure-independent (the peak intensities were linearly dependent on pressure), and a deconvoluted spectrum was used for each energy. As a check on random fluctuations, spectra taken at all four pressures at 50-keV primary energy were deconvoluted. Random fluctuations in the results obtained by either method were about $\pm 10\%$. No pressure dependence was observed.

Absolute total cross sections for the sum of the $1^1S \rightarrow 2^1P$ and $1^1S \rightarrow 2^1S$ transitions obtained by the above procedure are shown in Fig. 6. The error brackets are $\pm 20\%$ and represent total systematic and random errors to be discussed later. Resolution errors peculiar to the excitation cross sections are also covered by the error brackets. These arise from contributions from higher-order unresolved peaks.

Unresolved peaks contribute to the 21.36-eV peak when the high energy-loss side of the peak does not drop to zero. An estimate of the error involved was obtained by a graphical construction in which it was assumed that the ^1S and ^1P peaks in the actual differential cross sections could be represented by δ functions whose heights followed a n^{-3} law, where n is the principal quantum number of the level in question. This dependence has been

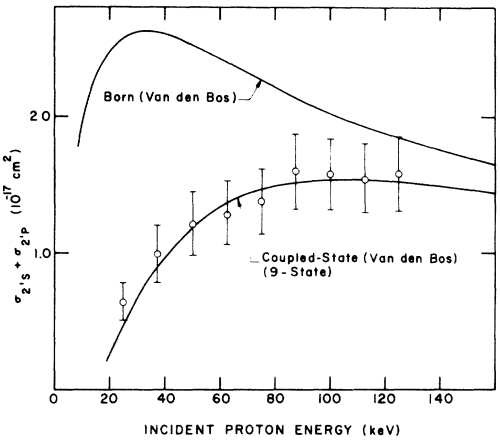

FIG. 6. Total cross sections for the Sum of the $1^1S \rightarrow 2^1S$ and $1^1S \rightarrow 2^1P$ transitions. Φ: present data. Born approximation is from Ref. 24; the coupled-state approximation is from Ref. 25.

observed experimentally by Van den Bos *et al.*[22] and derived by Ochkur and Petrunkin.[23] The resolution curve was then superimposed on these peaks and the ordinates added point by point. Varying contributions of 2^1S relative to 2^1P were introduced and the n^{-3} dependence was assumed for both n^1S and n^1P ($n = 3, 4, 5, 6$). States of higher principal quantum number, as well as ^1D states and above, were neglected. It was found that the height of the first peak is increased by about 2% when the minimum at the right side of the peak is 20% of the peak height, as in our deconvoluted spectra. A shift of up to +0.1 eV in the location of the peak was also noted, depending on the relative 2^1S and 2^1P contributions. This explains why the peak lies at a higher energy loss than corresponds to either the 2^1S or 2^1P levels.

Shown also in Fig. 6 are results of the Born and coupled-state approximation calculations of Van den Bos.[24,25] The theoretical results for excitation to the 2^1S and 2^1P states have been added to obtain the curves in Fig. 6. The coupled-state calculations are those reported in Ref. 25 for a 9-state expansion of the helium wave functions. The Born approximation, which is not valid at these energies, gives results which are factors of 2–3 above the data except at the higher energies. The coupled-state approximation gives excellent agreement at all but the lowest energy used in the present experiment. No experimental data are available for comparison with our results.

The cross sections shown in Fig. 6 are for the sum of the excitations to the 2^1S and 2^1P levels. Estimates of the relative contributions of each were obtained from several sources. Bates[26] has pointed out that on theoretical grounds the cross sections for the optically forbidden $1^1S \rightarrow 2^1S$ transition is expected to be smaller than that for the optically allowed $1^1S \rightarrow 2^1P$ transition. This conclusion is substantiated by experimental studies of the 4^1S and 4^1P excitation cross sections (and higher-order pairs).[22] Since the n^{-3} law applies to both S and P states, the relative magnitudes should be the same for all n.

Proceeding on this evidence, we have made careful studies of the leading edge of the 21.36-eV peak in our spectra, comparing it to results of the graphical convolution mentioned earlier. In the latter, varying percentages of 2^1S contribution were introduced into the graphs and the n^{-3} law was assumed for both the ^1S and ^1P peaks. Six such pairs of peaks were placed at the spectroscopic values of energy loss (see Ref. 18). A total of 36 spectra were analyzed in this way. The estimated contributions of the 2^1S state relative to the 2^1P state obtained in this study ranged from 0.1 at the high energies (> 100 keV) to unity at the low energies (25-50 keV), with an uncertainty of about 50 %. While this is a large uncertainty, the resulting uncertainty in the estimate of the 2^1P cross section is less. That is, if the ratio of the 2^1S contribution to the 2^1P contribution is f, the 2^1P cross section is $(1+f)^{-1}$ times the sum of the two and the fractional error due to the uncertainty in f is $\Delta f/(1+f)$.

Total cross sections for the $1^1S \rightarrow 2^1P$ transition obtained using our estimates of the relative contribution of the 2^1S to the 2^1P transition in the above procedure are shown in Fig. 7, together with results of the Born,[24,27] distortion,[28] and coupled-state[25] calculations. Data obtained using the $2^1S/2^1P$ ratio given by the theoretical results of Van den Bos,[24,25] together with our measurements of $\sigma_{2^1S} + \sigma_{2^1P}$, are consistent with that shown in Fig. 7. No other measurements of this

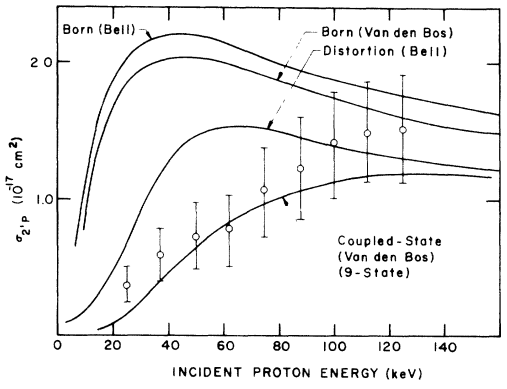

FIG. 7. Total cross sections for the $1^1S \rightarrow 2^1P$ transition. Φ: present data. The Born approximations are from Refs. 24 and 27; the distortion approximation is from from Ref. 28; the coupled-state approximation is from Ref. 25.

cross section are known to us. The present results are in good agreement with the coupled-state calculations of Van den Bos throughout the energy range, and with the distortion-approximation results at higher energies. There is no agreement with the distortion approximation below 87.5 keV. The Born approximation overestimates the cross section by factors of 2 - 3 at the lower energies.

VII. TOTAL IONIZATION CROSS SECTIONS

Total cross sections for ionization were obtained from both the raw and deconvoluted spectra. Integration of Eq. (3) over the continuum yields the ionization cross section directly from the raw spectra. Integration over the continuum in the deconvoluted spectra also yields the ionization cross section. No systematic differences were noted in the results obtained by the two methods. Results obtained at a given energy were therefore averaged.

Total cross sections for ionization of helium by protons are shown in Fig. 8, along with results from theory and other experiments. All the other experimental data shown in the figure were obtained by some variation of the parallel-plate condenser method wherein either ejected electrons or recoil ions were collected. Agreement among different investigators using that method is good except at lower energies.

The results of the classical calculation shown in Fig. 8 are factors of about 2 above the data, while the results of the Born approximation show better agreement but place the maximum at too low an energy.

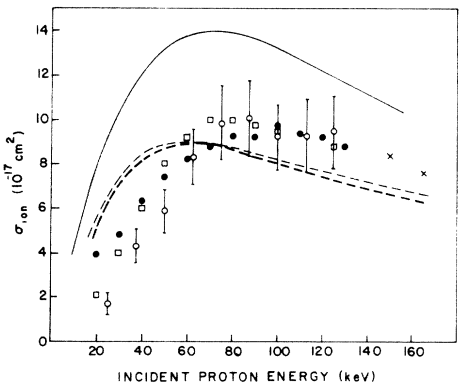

FIG. 8. Total ionization cross sections. Φ: present data; ● : data of DeHeer *et al.* (Ref. 4); □ : data of Federenko *et al.* (Ref. 3); *X*: data of J. W. Hooper *et al.*, Phys. Rev. 125, 2000 (1962); --- Born approximation, Mapleton (Ref. 30); — — — Born approximation, G. Peach, Proc. Phys. Soc. (London) 85, 709 (1965); —— classical theory, J. D. Garcia *et al.*, Phys. Rev. 165, 66 (1968).

The present data agree well with that of others, considering the fundamental differences in method. Our results do, however, show a faster decrease toward the lower energies than do the others. The main features agree most closely with the data of Federenko *et al.*[3]

There is no apparent reason why the present results should be any less reliable at the lower energies than over the rest of the range. Increased loss of beam by scattering at low energies is unlikely in view of the absence of any noticeable trend in experimental tests for large-angle scattering. The only errors peculiar to the ionization cross sections are those resulting from contributions from preionization peaks. A graphical construction similar to that employed in the case of the excitation cross sections indicates that if the integration for the total cross section is begun at the ionization limit, the contribution from the discrete part of the spectrum is nearly canceled by the corresponding loss from the continuum. In any case, the area in question is at most about 2% of the total area under the continuum with the present resolution.

In comparing our ionization cross sections with those obtained by the parallel-plate capacitor method, consideration must be given to the differences between the two methods insofar as contributions from processes other than first ionization are concerned.

All the data shown in Fig. 8 are reported as cross sections for first ionization; i.e., for the process

$$H^+ + He \rightarrow H^+ + He^+ + e .$$

In the parallel-plate method this process is identified by the appearance of a singly charged helium ion and one electron. In our method, it is identified by the appearance of a single continuum beginning at the first ionization potential in the energy-loss spectrum.

Second ionization

$$H^+ + He \rightarrow H^+ + He^{++} + 2e$$

would contribute double charges (in the absence of charge analysis) in the parallel-plate method, but would produce a second continuum, beginning at the second ionization potential, in the energy-loss spectrum in our method. The second continuum should be observable if second ionization contributed significantly to our results. No second continua were observed.

Charge exchange

$$H^+ + He \rightarrow H + He^+$$

contributes an ion, but no electron, and thus, should not be counted in the parallel-plate method. Charge exchange is not counted in our method either. The process produces a neutral projectile, which cannot negotiate the magnet or energy analyzer in our apparatus, and is therefore not detected.

Simultaneous ionization and charge exchange

$$H^+ + He \rightarrow H + He^{++} + e$$

contributes double positive charges in the parallel-plate method, but again produces a neutral projectile, which goes undetected in our method.

The consequences of simultaneous ionization and excitation,

$$H^+ + He \rightarrow H^+ + He^{+*} + e,$$

are the same in either method, as is also true for autoionization. In the parallel-plate method either process produces a singly charged ion and one free electron and is thus counted as first ionization. In our method, either process produces features in the energy-loss spectrum which are included in the integrations for the total ionization cross sections and are therefore counted as first ionization.

Secondary processes such as ionization by electrons ejected in the primary collision can add to the number of ions and free electrons in the collision chamber. They cannot, however, affect the energy lost by the projectile and so cannot contribute to our results.

Neutral particles in the beam can also produce ionization, which must be separated from that due to the protons in the parallel-plate method. As mentioned before, neutrals cannot contribute to the present results.

In summary, the results of the present study are for first ionization only, with preionization peaks, large-angle scattering, and second ionization being the possible complications. Of these, only the second could cause the cross sections to be lower at lower energies and this possibility has been eliminated with some confidence by the auxillary experiments discussed earlier. Of the processes discussed above which could make the results of the parallel-plate experiments higher than ours, those involving charge exchange or a neutral beam component would be expected to have more influence at the lower energies where the charge-exchange cross sections reach a maximum.

VIII. PARTIAL STOPPING POWERS

The partial stopping power ε_p of a substance toward a beam of protons is defined as

$$\varepsilon_p = (1/ndx)\,\bar{\xi},$$

where $\bar{\xi}$ is the average energy lost by those protons which have retained their identity as protons throughout the collision region. In contrast to the conventional total stopping powers, which are usually measured with high target-gas pressures where the beam is in charge equilibrium, partial stopping powers exclude losses from electron capture-and-loss cycles and from elastic effects due to multiple collisions.

Partial stopping powers are obtained in the present method by direct integration of the spectra. Any asymmetry in the incident-beam energy distribution is compensated for by subtracting the average of the distribution of the resolution curve from the average energy loss of the spectrum, viz,

$$\varepsilon_p = \frac{1}{ndx}\left(\frac{\int \xi R(\xi)\,d\xi}{\int R(\xi)\,d\xi} - \frac{\int \xi \Phi(\xi)\,d\xi}{\int \Phi(\xi)\,d\xi}\right).$$

Results of the partial stopping power measurements are shown in Fig. 9. Total stopping power data of Park and Zimmerman[29] are also shown for comparison. As expected, the present results lie considerably lower than the total stopping powers, the differences increasing at lower energies where charge exchange is more probable.

IX. TOTAL CROSS SECTIONS FOR INELASTIC PROCESSES

Total inelastic cross sections were obtained by integrating over the entire apparent differential cross-section curves. These were averaged with results obtained by integrating over the inelastic portion of the energy-loss spectra and dividing by the area under the resolution curve. The

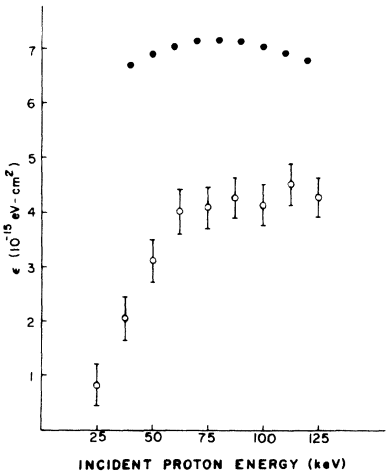

FIG. 9. Partial stopping powers. Φ: partial stopping powers (present data); ●: total stopping powers, Park and Zimmerman (Ref. 29).

errors in this procedure are essentially the same as those discussed in Sec. VIII on ionization cross sections except that resolution is not a factor. The results are shown in Fig. 10. Also shown in the figure are results of a rough Born approximation obtained by direct addition of results for the 1^1S-n^1P ($n = 2, 3 \cdots 6$) and the 1^1S-n^1D ($n = 3, 4, 5$) transitions obtained by Bell *et al.*,[27] the 1^1S-n^1S ($n = 2, 3, 4$) transitions obtained by Van den Bos,[24] and the total ionization cross section calculations of Mapleton.[30] Other excitation processes were considered negligible on the grounds that they are forbidden for proton impacts or that, from the trends noted in Refs. 24 and 27, they are several orders of magnitude lower than the processes considered. The agreement in Fig. 10 shows a pattern very similar to that shown in Fig. 8 for ionization cross sections.

X. ACCURACY

The error bars shown on the present data are a standard ±20%, with the exception of those on the $1^1S \rightarrow 2^1P$ data. In every case, this figure exceeds 2 standard deviations in the observed fluctuations and for some points is as much as 5 standard deviations. The error bars are thus conservative estimates. The estimated errors were arrived at through the analysis in Secs. X A–X C.

A. Random Errors

The recorded spectra were reproducible to within ±5%, which covers random fluctuations in all experimental parameters, including target-gas pressure, detection efficiency, and servo gains in the data-acquisition system. The integrated results for the total cross sections were reproducible to within ±10%. This figure covers random errors in all stages of the data reduction as well as the fluctuations noted above.

B. Systematic Errors

1. *Pressure*

The target-gas pressure was measured by an MKS Baratron type 77 capacitance bridge manometer,[31] which was calibrated against a CVC-type Gm-100A mercury McLeod gauge.[32] The calibration yielded a slope of

$$P_{\text{Baratron}}/P_{\text{McLeod}} = 1.17 \pm 0.01.$$

The scales for the cross sections have been adjusted accordingly and the uncertainty in the slope retained as a systematic error. Since the McLeod gauge was the laboratory standard, errors inherent in that gauge could not be determined directly. Utterback[33] has found a 2% error in the case of helium under experimental conditions very similar to those of the present experiment. Because of this possible error and the error involved in the calibration, a total uncertainty of 5% has been assigned to the pressure measurement.

In view of the considerable calibration discrepancy between the two gauges, it is possible that an unknown error exists in the pressure measurement. Such an error could necessitate an upward shift of all the results by 17% if the Baratron were taken as the laboratory standard. The data points would still fall within the 20% error brackets.

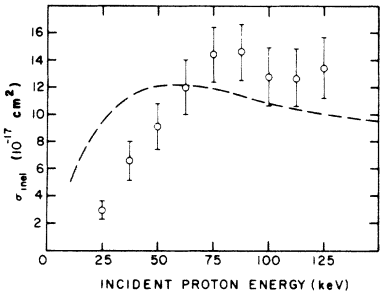

FIG. 10. Total inelastic cross sections. Φ: present data; --- composite Born approximation.

2. *Angular Scattering*

An evaluation of the effects of scattering beyond the acceptance angles was given earlier. As was indicated there, estimates of the amount of beam scattered out averages 3%. However, since the estimates showed both positive and negative fluctuations and since no trend with energy was found, no corrections were made to the data. The results are, therefore, uncertain by 3% due to scattering.

3. *Multiple Scattering*

When the pressure in the target chamber is increased to where multiple collisions are probable, repetitions of the single-collision spectra at energy losses corresponding to the order of multiplicity of the collisions are noted. The range of target-gas pressures was chosen well below pressures where such repetitions were observed.

A further test of the prevalence of single-collision conditions is provided by a study of the linearity of the pressure dependence of the scattered beam intensity. For this study, the most intense peak in the spectra, the 21.36-eV peak, was chosen. A plot of the intensity of this peak relative to that of the resolution curve is shown in Fig. 11. It is evident from this plot that the present operating range is well down into the single-collision region. Therefore, errors from multiple scattering are considered to be negligible.

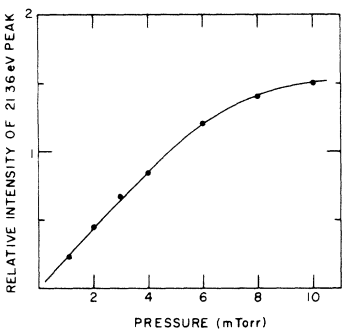

FIG. 11. Pressure dependence of the 21.36-eV peak.

4. *Scattering Path Length*

The scattering path length dx was taken to be the accurately measured length of the target chamber (6.345 ± 0.003 cm). The pressure in the differential pumping regions outside the target chamber remained at the system pressure under operating conditions. At much higher target-gas pressures (up to 100 μ) the pressure in the differential pumping region was a factor of about 10^{-3} that in the target chamber. Hence no correction was made for gas in the differential pumping region and it was considered that errors resulting from the differential pumping could be neglected.

5. *Spectral Energy Scale*

The spectral energy scale (x axis of the recorder) was periodically calibrated against ΔV. The slope of the calibration curve was corrected to

$$\Delta V/\Delta V_{\text{Readout}} = 10.0,$$

with each calibration, the correction never amounting to more than 1% of ΔV. This is consistent with the fluctuations noted in the location of the primary energy-loss peak in the spectra.

6. *Primary Energy Scale*

The accelerating voltage was determined by measuring the drop across a voltage divider composed of 0.5% tolerance resistors. The measurement was made on a differential voltmeter having an accuracy of 0.02%. The primary energy scale is believed to be accurate to within ±0.6%.

C. Summary of Errors

The estimated systematic errors discussed above were added vectorially. The result was added algebraically to the random error to obtain an estimate of the total uncertainty.

The results for the various cross sections were as follows: ±12% for the apparent differential (exclusive of resolution errors); ±19% for the sum of the 2^1S and 2^1P excitations; ±33% for the 2^1P excitation (including estimated error in separating the 2^1S and 2^1P peaks); ±16% for total ionization; and ±15% for total inelastic and stopping powers.

XI. CONCLUSIONS

The method used in this experiment can provide the cross section for any collisionally induced inelastic process which can be unambiguously identified with a definite energy transfer and which does not involve a change of charge of the incident ion. The method is subject to several limitations.

We have discussed the effects of angular scattering. These limit application of the method wherever there is reason to suspect large cross sections for certain processes at large scattering angles. Measurements of the energy-loss spectra as a function of angle would thus be desirable and may prove necessary for heavy target systems. Modifications to include direct angular measurement capabilities are under study.

A more severe limitation is imposed by the need for high resolution in the energy-loss spectra. If the resolution is inadequate, proper interpretation of the observed spectra may become quite difficult in all but the simplest target systems. If the energy levels of the target system are known, then the identity of most peaks in the spectra can be established by reference to the selection rules associated with the projectile system. However, as has been found in this experiment, lack of resolution can result in apparent shifts of unresolved lines, thereby introducing uncertainties in the identifications.

It should be noted that although the differential cross sections obtained by the present method are labeled "apparent," total cross sections obtained by integrating over a resolved peak are absolute in the sense that they are not normalized to results of theory or other experiments. The measurements are independent of apparatus calibrations and depend only on the short-term stability of the apparatus constants. As is true in all experiments with gaseous targets, the cross sections depend on the absolute measurement of the target-gas pressure and the effective path length of the ion in the gas.

In general, where theory or experiments were available for comparison, the agreement with our method is satisfactory. With respect to the differential cross sections themselves, the only discriminating comparisons are with ejected electron energy distributions. Here, the observed differ-

ences are consistent with expectations based on studies of the differences between the two experiments.

Because of the inability to resolve the 2^1S peak, the measurement of the $1^1S \rightarrow 2^1P$ excitation cross section is dependent on the ratio of the contributions from the two processes. Since the ratio is difficult to determine, the $1^1S \rightarrow 2^1P$ excitation cross sections have a larger uncertainty than the other measurements. This uncertainty is not, however, unusually large for an excitation measurement and the agreement with theory is very satisfactory.

The total cross sections for the sum of the excitations to the 2^1S and 2^1P states involve only a small resolution error and thus provide a positive test of the recent coupled-state calculations. The agreement obtained in this case is quite exceptional for an excitation cross section.

The purpose of this experiment was to study the feasibility of measuring certain fundamental collision cross sections by means of an energy analysis of the primary beam particles. We have demonstrated that differential cross sections for protons on helium can be obtained from a study of the energy-loss spectra of the forward scattered beam. The good agreement obtained in the case of total ionization cross sections is evidence of the basic soundness of the method.

ACKNOWLEDGMENTS

The authors would like to express their thanks to Donald R. Schoonover and Graham Hale for their assistance in taking the data, to Charles Myles for devising the computer program and to Ron Maehl for assisting with the data reduction. We deeply appreciate the cooperation and helpful suggestions made by the members of the UMR Physics staff. We are very grateful for the Research Corporation grant which initiated this research project and for the continued support of the National Science Foundation.

APPENDIX

A simple iterative procedure was used for numerical deconvolution of the experimental integral equation [Eq. (1)]. Denoting the convolution operation by an asterisk (*); i.e.,

$$f * g \equiv \int f(x-y)g(y)\,dy,$$

the equation becomes

$$R = T * \Phi,$$

where $T = ndx\frac{d\sigma}{d\xi}$.

The following iteration scheme was used

$$T_0 = R - \kappa\Phi / \int \Phi(\xi)\,d\xi,$$

$$T_n = \frac{T_{n-1}}{\int \Phi(\xi)\,d\xi}\left[(R - \kappa\Phi)/R_{n-1}\right] * \Phi,$$

where $\kappa = R(0)/\Phi(0)$,

and $R_n = T_n * \Phi$.

In this scheme, the resolution curve is first scaled to the elastic peak of the spectrum and then subtracted from the spectrum to remove the background. The result is then divided by the area under the resolution curve to obtain an initial estimate T_0, for T. This estimate is then convoluted with Φ to obtain a comparison function, R_n, for R. The resulting R_n is compared to $R - \kappa\Phi$ by calculating the sum of the squared deviations between each pair of points on the two curves. If the sum is not within a prescribed range, T_0 is corrected to yield T_1, and the procedure is iterated until the prescribed degree of accuracy is obtained.

The process has proven very stable and usually converges to $R_n = R - \kappa\Phi$ to within 0.1% after 20 iterations.

---

†Work supported through a grant from the National Science Foundation.

[1]H. B. Gilbody and A. R. Lee, Proc. Roy. Soc. (London) 274A, 365 (1963).

[2]H. B. Gilbody, J. B. Hasted, A. R. Lee, J. V. Ireland, E. W. Thomas, and A. S. Whiteman, Proc. Roy. Soc. (London) 274A, 40 (1963).

[3]N. V. Federenko, V. V. Afrosimov, R. N. Il'in, and E. S. Solov'ev, Proceedings of the Fourth International Conference on Phenomena in Ionized Gases (North-Holland Publishing Co., Amsterdam, 1960), Vol. IA, p. 47.

[4]F. J. DeHeer, J. Schutten, and H. Moustafa, Physica 32, 1766 (1966).

[5]H. W. Berry, Phys. Rev. 127, 1634 (1962).

[6]C. E. Kuyatt and T. Jorgensen, Jr., Phys. Rev. 130, 1444 (1963).

[7]M. E. Rudd, C. A. Sautter, and C. L. Bailey, Phys. Rev. 151, 20 (1966).

[8]W. L. Fite, in Atomic and Molecular Processes, edited by D. R. Bates (Academic Press Inc., New York (1962), p. 421.

[9]F. J. DeHeer, in Advances in Atomic and Molecular Physics, edited by D. R. Bates (Academic Press Inc., New York, 1966), p. 327.

[10]M. DuFay, J. P. Buchet, M. Carre, A. Denis, J. Desesquelles, and M. Gaillard, Proceedings of the Fifth International Conference on Physics of Electronic

and Atomic Collision (Nauka Publishing House, Leningrad, 1967), p. 295.
[11]H. R. Moussa, H. R. Moustafa, and F. J. DeHeer, Physica 36, 646 (1967).
[12]E. W. Thomas and G. D. Bent, Phys. Rev. 164, 143 (1967).
[13]J. T. Park and F. D. Schowengerdt, Rev. Sci. Instr. 40, 753 (1969).
[14]P. M. Stier and C. F. Barnett, Phys. Rev. 103, 896 (1956).
[15]R. A. Mapleton, Phys. Rev. 122, 528 (1961).
[16]M. Barat and J. C. Houver, Compte Rendu 264B, 38 (1967); 264B, 296 (1967).
[17]H. Boersch, J. Geiger, and B. Schröder, Proceedings of the Fifth International Conference on Physics of Electronic and Atomic Collisions (Nauka Publishing House, Leningrad, 1967).
[18]E. N. Lassettre, A. S. Berman, S. M. Silverman, and M. E. Krasnow, J. Chem. Phys. 40, 1232 (1963).
[19]M. E. Rudd, Phys. Rev. Letters 13, 503 (1964).
[20]M. E. Rudd and T. Jorgensen, Jr., Phys. Rev. 131, 666 (1963).
[21]J. D. Garcia, Phys. Rev. 177, 223 (1969).
[22]J. Van den Bos, G. J. Winter, and F. J. DeHeer, Physica 40, 357 (1968).
[23]V. I. Ochkur and A. M. Petrunkin, Opt. i Spektroskopiya 14, 457 (1963) [English transl.: Opt. Spectry. (USSR) 14, 245 (1963)].
[24]J. Van den Bos, Physica 41, 678 (1969).
[25]J. Van den Bos, Phys. Rev. 181, 191 (1969).
[26]D. R. Bates, Atomic and Molecular Processes (Academic Press Inc., New York, 1964), p. 590.
[27]K. L. Bell, D. J. Kennedy, and A. E. Kingston, Proc. Phys. Soc. (London) [J. Phys. B1, 218 (1968)].
[28]R. J. Bell, Proc. Phys. Soc. (London) 78, 903 (1961).
[29]J. T. Park and E. J. Zimmerman, Phys. Rev. 131, 1611 (1963).
[30]R. A. Mapleton, Phys. Rev. 109, 1166 (1958).
[31]MKS Instruments, Inc., Burlington, Mass.
[32]Consolidated Vacuum Corp., Rochester 3, N. Y.
[33]N. G. Utterback and T. Griffith, Jr., Rev. Sci. Instr. 37, 866 (1966).

PHYSICAL REVIEW VOLUME 185, NUMBER 1 5 SEPTEMBER 1969

X-Ray Production in C^+ - C Collisions in the Energy Range 20 keV to 1.5 MeV*

R. J. Fortner, B. P. Curry, R. C. Der, T. M. Kavanagh, and J. M. Khan
Lawrence Radiation Laboratory, University of California, Livermore, California 94550
(Received 20 February 1969)

Cross sections for carbon K-x-ray production for C^+ ions incident upon a carbon target have been measured in the energy range 20 keV–1.5 MeV. A theoretical model based on the Landau-Zener theory of level crossing is formulated and is found to fit the experimental data within experimental uncertainty.

I. INTRODUCTION

In a previous paper,[1] cross sections for carbon K-x-ray production have been measured for heavy ions incident on a carbon target in the energy range from 20 to 80 keV. It was found that the cross sections are several orders of magnitude larger than those predicted by direct scattering theory. It was suggested that the mechanism for electron excitation was level crossing, as proposed by Fano and Lichten[2] to explain the results of Kessel and Everhart[3] for Ar^+-Ar collisions. An extensive discussion of the level-crossing mechanism is found in Ref. 4. As reported below, the data for C^+ ions incident on carbon are extended to 1.5 MeV, and a theoretical model based on the level-crossing mechanism is formulated and compared with the experimental data.

II. Experimental Measurements

The experimental techniques were essentially those described in earlier papers on protons.[5] A thick carbon target was used, and carbon K-x rays were detected by a gas-flow proportional counter with a $\frac{1}{4}$- or $\frac{1}{2}$-mil Mylar window. The directly measured quantity in these experiments was the number of detected x rays per unit charge incident upon the target. The thick-target yield I (x rays per ion) was obtained by bombarding the carbon target alternately with protons and C^+ ions and normalizing to the known carbon x-ray yield